Journal of Energy Storage 101 (2024) 113764

Contents lists available at ScienceDirect

Journal of Energy Storage

journal homepage: www.elsevier.com/locate/est

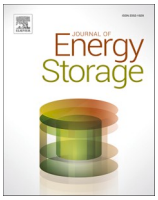

Research Papers

Stabilization of reactive bed particles for thermochemical energy storage with fiber reinforcement

A. Shkatulov [a,b], E. Averina [b,c], T. Raemaekers [b], H. Fischer [d], O.C.G. Adan [b,c], H. Huinink [b,c,*]

[a] Iberian Center for Research in Energy Storage, CIIAE, 10003 Cáceres, Spain
[b] Eindhoven University of Technology, Den Dolech 2, Eindhoven, 5600, MB, Netherlands
[c] Eindhoven Institute for Renewable Energy Systems, Eindhoven University of Technology, PO Box 513, Eindhoven, 5600, MB, Netherlands
[d] TNO Materials Solutions, High Tech Campus 25, Eindhoven, 5656, AE, Netherlands

ARTICLE INFO

Keywords:
Thermochemical energy storage
Salt hydrates
Composites
Stabilization
Packed bed reactor
Polymer fiber reinforcement

ABSTRACT

Thermochemical energy storage (TCES) is an emerging technology harnessing chemical reactions for storage of thermal energy. Among the primary challenges for TCES based on crystal-to-crystal chemical transformations is the design and manufacturing of macroscopic reactive particles that are resistant to mechanical changes over multiple cycles of operation. Such changes often lead to an increase in the pressure drop over a packed bed, thereby adversely affecting the performance of TCES. This work explores the effect of polymeric fibers on reactive TCES particles as a potential route for mechanical stabilization of both the particles and the bed. The salt hydrate $K_2CO_3{\cdot}1.5H_2O$ was used as a model thermochemical material and polyacrylonitrile fibers (PAN) were selected as a reinforcing additive. The stabilization effect of fibers for composite tablets of ($K_2CO_3{\cdot}1.5H_2O$)#PAN with respect to crushing behavior, salt deliquescence and deformation after 50 cycles was demonstrated and attributed to the shape-stable structures formed by the internal fiber networks. The increase of a pressure drop at a reactive bed of fiber-reinforced particles was found to be smaller by a factor of 1.5–3 as compared to a bed of pure K_2CO_3 tablets, while the reaction rate was unaffected. Thus, the proposed approach may be an inexpensive and efficient route to stable macroscopic reactive particles for TCES reactors.

1. Introduction

The modern challenges of decarbonization and sustainable development call for affordable and clean energy [1]. As thermal energy accounts for >50% of the final energy consumption [2,3], the means of efficient storage, upgrade and reallocation of thermal energy are of paramount importance to reach this goal. Thermal energy storage is especially beneficial in regions with good availability of renewable energy sources, e.g. solar energy [4].

Harnessing reversible chemical reactions for heat storage - or **T**hermo**C**hemical **E**nergy **S**torage (TCES) – is gaining momentum due to the unique features of this technology such as high energy storage density and long duration [5], along with the possibility of thermal upgrade and general versatility of thermal management toolbox offered by TCES [6]. These advantages make the technology promising for thermal energy storage in a built environment, including space heating [7]. The most investigated TCES is based on the sorption/desorption of water. Along with adsorption on a surface [8] or absorption in solutions [9], capturing water molecules in crystalline solids to form crystalline salt hydrates is considered a promising way towards compact and inexpensive TCES units for residential heating [10,11]. A TCES system based on the transformations of salt hydrates is charged by dehydrating a hydrate with release of water vapor:

$$Salt{\cdot}nH_2O_{(cr)} \leftrightarrows Salt{\cdot}(n-m)H_2O_{(cr)} + mH_2O_{(gas)} \quad (1)$$

and discharged by carrying out the backward reaction when and where the stored heat is needed. For many salt hydrates reaction (1) possesses thermodynamic properties suitable for domestic applications ($\Delta_r H^o$ = 50–75 kJ/mol, $\Delta_r S^o$ = 140–160 J/mol/K, maximal storage density > 1 GJ/m^3 [12]) which allows charging at T = 100-150°C and discharging at target temperatures T = 40-70°C. Therefore, the class of salt hydrates is potentially useful for space heating or hot water generation. Currently, several salt hydrates have been proposed for domestic TCES [10,12–17], the selection in each case depends on the quality of source/sink, the T-p operational windows of the desired processes and non-technical considerations such as material price, toxicity, etc.

* Corresponding author at: Eindhoven University of Technology, Den Dolech 2, Eindhoven, 5600, MB, Netherlands.
E-mail address: h.p.huinink@tue.nl (H. Huinink).

https://doi.org/10.1016/j.est.2024.113764
Received 11 March 2024; Received in revised form 3 September 2024; Accepted 8 September 2024
Available online 18 September 2024

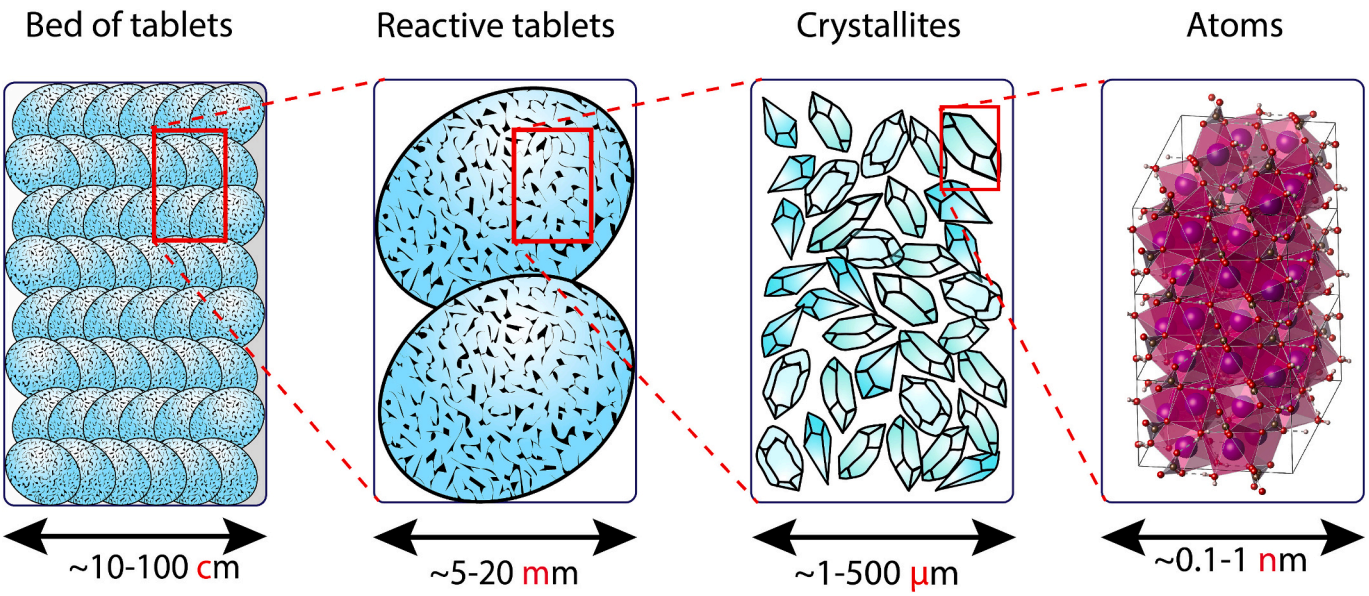

Fig. 1. Hierarchical structure of a material in thermochemical system along with the typical length scales.

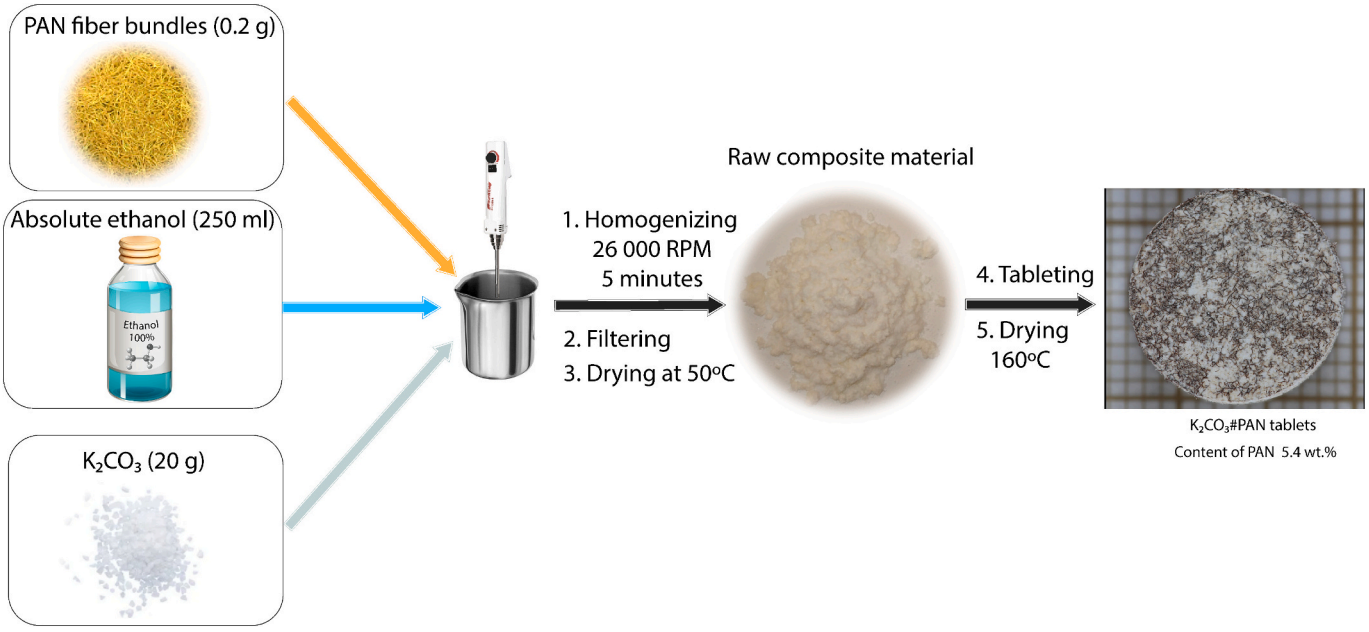

Fig. 2. Schematic preparation of the composites K_2CO_3#PAN.

A reactive bed of particles is the core of a TCES system. One of the variants considered technically sound for domestic-scale TCES units is a bed consisting of ~0.5–2 cm particles (tablets or granules) to avoid large pressure drop [18] or provide good mass flowability and particle durability for moving beds [19]. These tablets must be manufactured from primary crystallites of the salt that are usually much smaller (1–500 μm), and stability on the tablet level must be ensured, which is usually achieved by using binders [20] or porous matrices [21]. Finally, the crystallites consist of periodic arrangements of atoms (usually <10 nm in size) intermitted by one-, two- and three-dimensional defects. The hierarchy of the TCES system on material level is depicted in Fig. 1.

One of the major challenges on the way to practical application of salt hydrates is stabilization on the levels of reactive tablets and bed. Repetitive dehydration/hydration may cause degradation of the bed due to cracking of primary crystallites in the course of dehydration (charging) and agglomeration due to surface mobility in the course of hydration. Such repetitive cycling usually leads to either pulverization or agglomeration of the crystallites which also affects mechanical properties of the reactive tablets and the bed. Overall, the irreversibility of dehydration and rehydration manifests itself in morphology changes akin to the ones that cause salt weathering [22] and often adversely affects mass transfer and performance of TCES systems [23]. Additionally, many salt hydrates are prone to deliquescence if relative humidity exceeds a threshold, which may cause destruction of the bed and clogging of a reactor.

The major route to stabilizing crystallites is putting them in a porous matrix with hydrophilic submicrometer-sized pores. These pores help to hold salt solution, which allows for recrystallization of salt crystallites during each thermochemical cycle given that the deliquescence threshold is exceeded during hydration. The pore volume must be large enough to accommodate crystals and/or solution, and to allow for high salt loading for storage applications. The typical examples of matrices

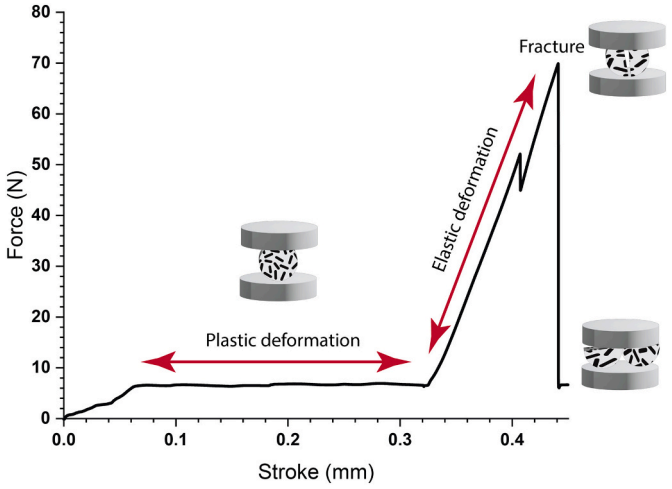

Fig. 3. A typical mechanical stability test of a K_2CO_3 tablet.

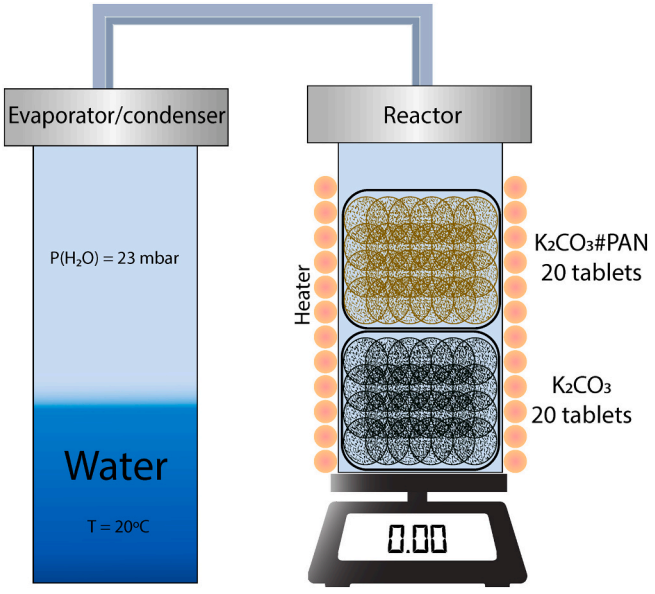

Fig. 4. Schematic representation of the PT-mass setup used for cycling.

include natural perlite [24], vermiculite [25], sepiolite [26], silica [27], zeolites [28], polymeric foams [29,30]. The recrystallization of a salt hydrate during each cycle stabilizes the sorptive and mechanical behavior of macroscopic centimeter-sized particles. Moreover, the salt deliquescence and absorption release extra heat at a lower temperature [31]. However, the use of porous matrices introduces a trade-off between efficient energy storage density and the temperature lift during discharging [32,33].

A potential alternative to traditional composites such as "salt/mineral matrix" or core-shell structures "salt@capsules" is tablets of salt crystallites reinforced by fibers creating a stabilizing skeleton in a new "salt#fibers" composite. Such a reinforcement technique is used in the building industry to boost the mechanical stability of concrete [34,35], however, it has never been investigated for application in TCES. The attractiveness of using fibers for TCES composites may be justified by typically low volumetric content of the fibers which could conserve the storage density and allow for potential scalability of manufacturing.

In this work, we investigate salt#fibers composites at the scales of a single tablet and a bed of tablets to elucidate the effect of fiber networks with respect to (a) deliquescence, (b) shrinkage/swelling and porosity, (c) reaction kinetics, and (d) evolution of bed pressure drop during cycling. Dehydration of potassium carbonate sesquihydrate was selected as a model TCES process as it was shown to be promising for domestic applications [10,36] due to low cost, low toxicity and favourable thermodynamic parameters of reaction

$$K_2CO_3{\cdot}1.5H_2O_{(cr)} \leftrightarrows K_2CO_3{\cdot}1.5H_2O_{(cr)} + 1.5H_2O_{(gas)} \quad (2)$$

On the other hand, the salt experiences shrinkage/swelling during cycles [23,25] and can be readily put into deliquescence at RH > 43%. The polymeric fibers made of polyacrylonitrile were selected for the reinforcement due to their hydrophilic surface, elasticity, low cost and availability as a concrete reinforcement material.

2. Experimental part

2.1. Material and tablets preparation

For preparing the "salt#fibers" composite we selected K_2CO_3 and polymeric fibers based on polyacrylonitrile (PAN) due to non-toxicity, mechanical properties suitable for reinforcement [37] and good thermal stability (Fig. S1 provided in Supplementary Material).

The K_2CO_3#PAN composite particles were prepared from dry K_2CO_3 (Evonik) and PAN fibers (Buddy Rhodes AC50, length 6 mm, thickness 12-15 μm) that were used as supplied. For preparation, the fiber bundles (1 g) were mechanically treated in absolute ethanol (~250 ml) in a stainless steel beaker by means of high-power homogenizer Kinematica POLYTRON 1200E equipped with a 12 mm dispersing aggregate (PT-DA 12/2EC-E157) rotating at 26 000 rpm for ca. 5 min to produce a viscous wool-like substance (Fig. 2). After the treatment of the fiber bundles, the crystalline particles of preliminarily dried K_2CO_3 (20.0 g in total, dried at 160°C overnight) were slowly added to the slurry of fibers in ethanol, which was followed by further homogenization for 5 min at 26,000 rpm. After the homogenization, the viscous slurry was quickly filtered with a paper filter on a vacuum filtration setup and dried at 50°C overnight, which resulted in raw material for tablets preparation (Fig. 2).

The tablets of K_2CO_3#PAN were prepared from the raw composite material (500 mg) by means of pressing with a stainless steel mold (12.3 mm in diameter and 2.4 mm in thickness) at $P = 20$ MPa for 30 s (column press PO-Weber PW-40 2). For comparison, the tablets of pure K_2CO_3 were pressed from the dried K_2CO_3 (Evonik). The pressed tablets were then dried for 48 h in an oven at 160°C. The fiber content in the final K_2CO_3#PAN tablets was determined independently by burning out the fibers at 700°C in air for ~5 h and dissolution of salt (see below), 4 tablets K_2CO_3#PAN were used in each experiment. By both methods it was shown that the fiber weight content ω_f in every experiment was 5.4 ± 0.5%.

To obtain the fiber residues of tablets, several dissolution tests were carried out by dissolving K_2CO_3 from the activated tablets K_2CO_3#PAN in large volume of water (250 ml per tablet) for 15 h. The residues were dried at room temperature in air. Thermal stability of the fibers was examined by FTIR spectroscopy (Fig. S3 provided in Supplementary Material).

2.2. Characterization methods

2.2.1. Individual tablet properties

Scanning electron microscopy images were captured using an electron microscope FEI Quanta 600 at 2–10 kV with a secondary electron detector. Samples were immobilized on a carbon-taped aluminum stage, quickly placed in the microscope chamber to minimize air exposure, and the chamber was then vacuumed to 3×10^{-5} mbar.

Porosity of the tableted particles in dehydrated (ε_d) and hydrated (ε_h) states was determined from weight m, weight content of the salt ω_h and ω_d in hydrated and dehydrated tablets, respectively and geometric parameters (diameter d and thickness t) measured by means of a digital caliper (Mitutoyo). The calculation was carried out as follows:

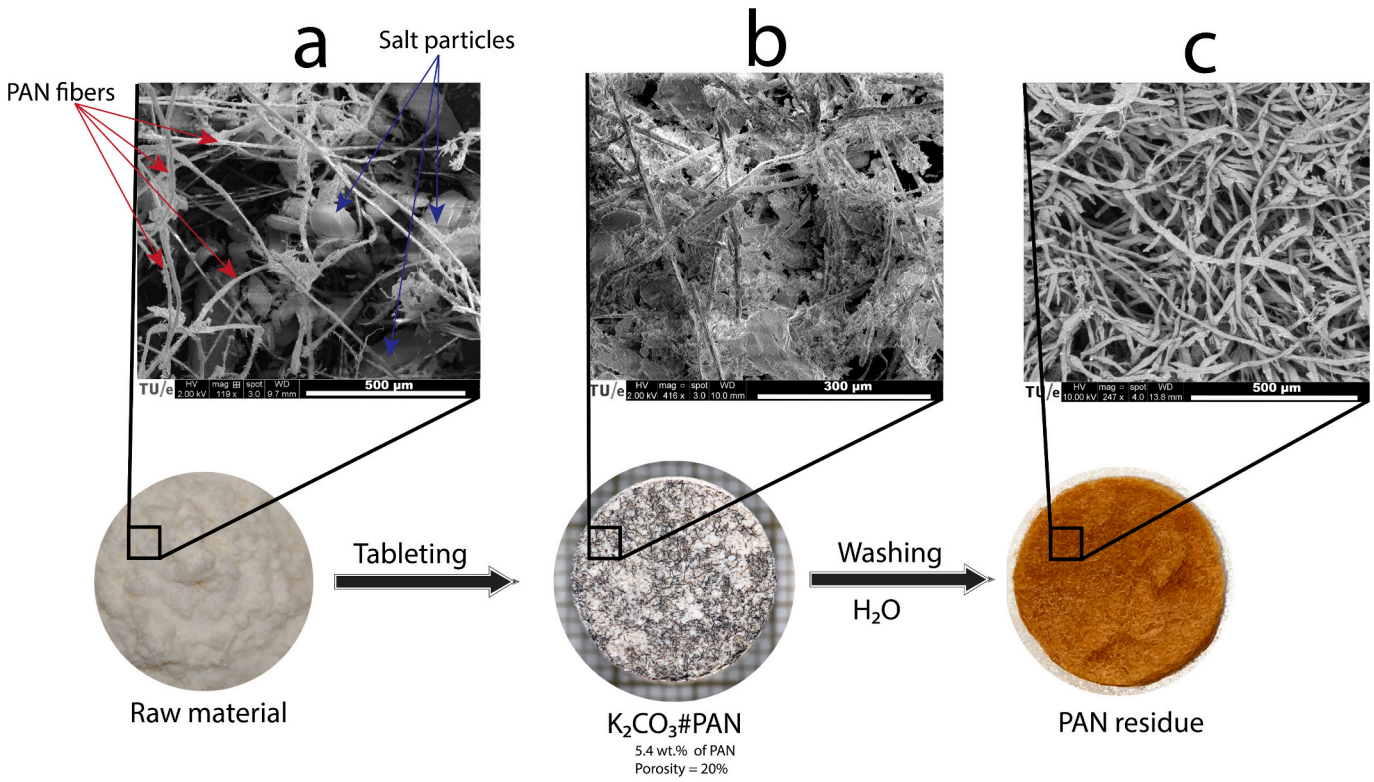

Fig. 5. The SEM images illustrating the macroscopic structure of the base material (a), pressed tablet (b) and entangled fiber residue after washing out of the salt (c).

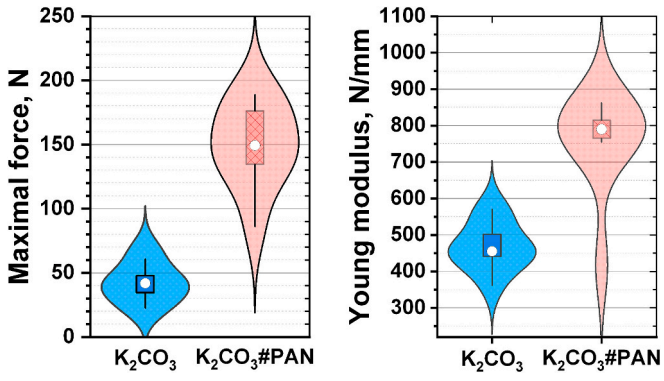

Fig. 6. Young modulus and maximal force observed during the tablet crushing tests. The white dots on violin plots show mean values, while the boxes show the 25–75% interval.

$$\varepsilon_h = 1 - \frac{V_{skeletal}}{V_{apparent}} = 1 - \frac{\frac{m\omega_h}{\rho_h} + \frac{m(1-\omega_h)}{\rho_f}}{\pi\left(\frac{d}{2}\right)^2 t} = 1 - 4\frac{m\left[\omega_h + (1-\omega_h)\frac{\rho_h}{\rho_f}\right]}{\pi\rho_h d^2 t} \quad (3)$$

$$\varepsilon_d = 1 - \frac{V_{skeletal}}{V_{apparent}} = 1 - \frac{\frac{m\omega_d}{\rho_d} + \frac{m(1-\omega_d)}{\rho_f}}{\pi\left(\frac{d}{2}\right)^2 t} = 1 - 4\frac{m\left[\omega_d + (1-\omega_d)\frac{\rho_d}{\rho_f}\right]}{\pi\rho_d d^2 t} \quad (4)$$

taking into account bulk densities of the salt (ρ_h = 2.18 g/cm^3 for $K_2CO_3{\cdot}1.5H_2O$ and ρ_d = 2.43 g/cm^3 for K_2CO_3 [24,25]) and bulk density of PAN (1.18 g/cm^3) and

$$\omega_d = 1 - \omega_f = 1 - \frac{5.4}{100} = 0.946 \quad (5)$$

$$\omega_h = \frac{\omega_d\frac{M_{K_2CO_3\cdot 1.5H_2O}}{M_{K_2CO_3}}}{\omega_d\frac{M_{K_2CO_3\cdot 1.5H_2O}}{M_{K_2CO_3}} + \omega_f} = \frac{\omega_d M_{K_2CO_3\cdot 1.5H_2O}}{\omega_d M_{K_2CO_3\cdot 1.5H_2O} + \omega_f M_{K_2CO_3}} = 0.954 \quad (6)$$

where M_S is a molar mass of salt S (S = K_2CO_3 or $K_2CO_3{\cdot}1.5H_2O$).

The porosity was measured for two series of K_2CO_3 and K_2CO_3#PAN composed of four tablets each. The tablets were subjected to repetitive hydration/dehydration cycles. The dehydration was carried out in a drying oven at 130°C while hydration was carried out in a desiccator over the saturated solution of $MgCl_2$ at room temperature (RH = 33%, P ~ 10 mbar). Both dehydration and hydration took 8–10 h to complete, and the full conversion was ensured by weight loss or gain. In total, 5 cycles were carried out for each tablet.

Reaction kinetics of hydration was measured *ex situ* by putting the dry single tablets of both K_2CO_3 and K_2CO_3#PAN into a desiccator over a saturated $MgCl_2$ solution which maintained partial water vapor pressure P(H_2O) at 10 mbar and 25°C (relative humidity 33% [38]) by forced convection. The weight *w(t)* at a certain moment *t* was recorded by briefly taking a tablet out from the desiccator and putting it back immediately after weighing. The kinetic curves were derived from periodic weighing of each tablet, then calculating conversion α of reaction (2) as follows:

$$\alpha(t) = \frac{w(t) - w(0)}{w(\infty) - w(0)} \quad (7)$$

where w(t) is weight of a tablet at moment t, w(0) is the weight of a dry tablet and w(∞) was calculated from the reaction stoichiometry and content of the salt ω:

$$w(\infty) = \omega_d\frac{w(0)}{M_{K_2CO_3}}M_{K_2CO_3\cdot 1.5H_2O} \quad (8)$$

for hydration and dehydration, respectively. For measuring dehydration kinetics, fully hydrated tablets were put in an oven at 130°C. In total, four tablets of K_2CO_3 and K_2CO_3#PANwere characterized

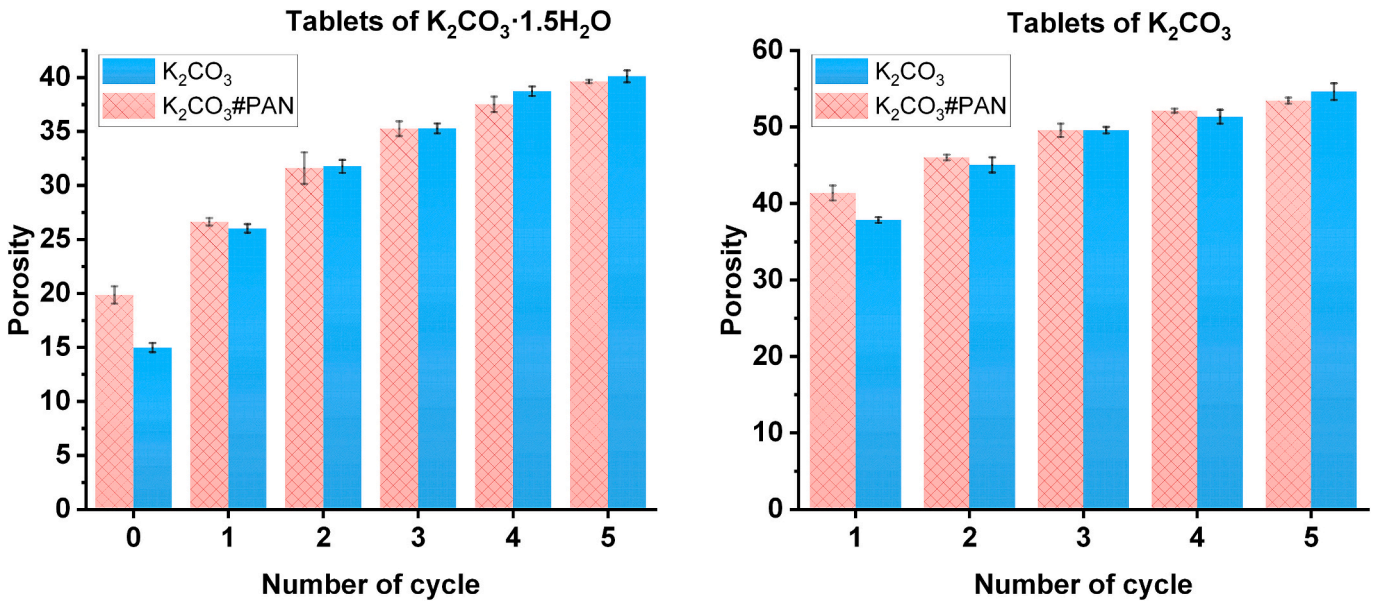

Fig. 7. Porosity for hydrated (left) and anhydrous (right) tablets of K_2CO_3 in comparison with K_2CO_3#PAN.

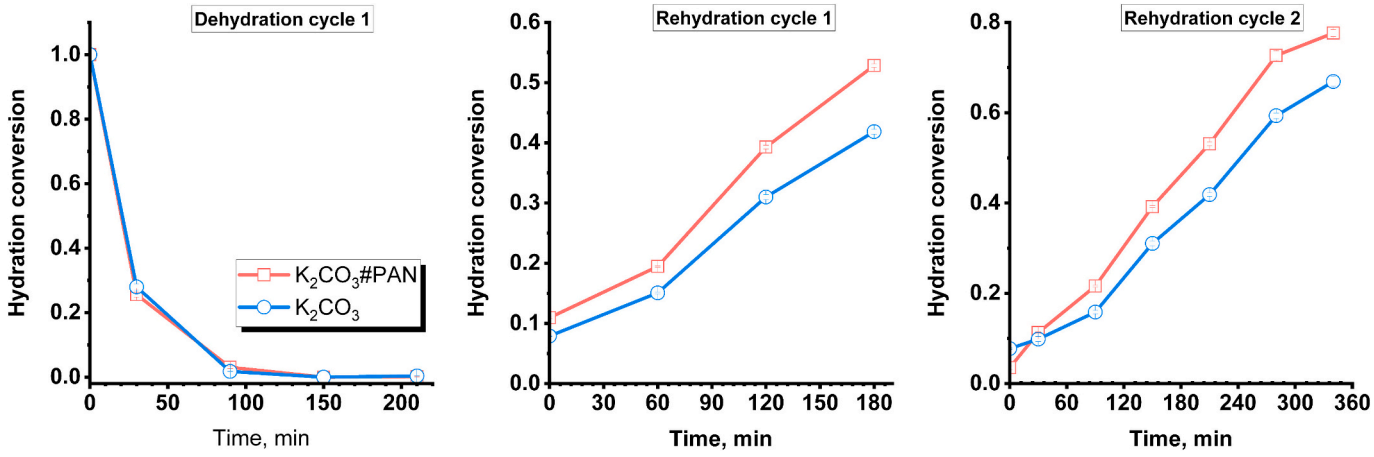

Fig. 8. Kinetic curves comparing dehydration (left) and rehydration (center, right) of K_2CO_3 and K_2CO_3#PAN tablets.

simultaneously, the kinetic curves were averaged.

Mechanical stability of tablets was investigated by using a Shimadzu AGS-X autograph equipped with spherically seated compression plates for testing compression strength. The cylindric tablets were put perpendicularly to the compression plane (Fig. 3). The stroke increasing at a rate of 0.25 mm/min was applied, and the force between the plates was registered by a force sensor with the limit of 200 N. Once the compression force sharply reduced by >10%, or when the stroke/force limit (0.5 mm/200 N) was achieved, the measurement was stopped. The two main characteristics were recorded, namely, the maximum crushing strength (even in the case of several cracking peaks) and the Young modulus, i.e. the initial slope of elastic deformation in Fig. 3. Two series of samples with and without fibers (10 tablets each) were measured.

Deliquescence tests were carried out for K_2CO_3#PAN by putting the tablets in the desiccators with saturated solutions of salts ($MgCl_2$, K_2CO_3, $Mg(NO_3)_2$, $NaNO_2$, NaCl) overnight at room temperature. All the desiccators in all the experiments were equipped with fans to force air convection inside.

2.2.2. Bed properties

Bed cycling was performed in a closed setup described in detail elsewhere [25,39], that consisted of a tube reactor of ca. 200 ml put on a balance and connected via flexible tubing to a thermostated evaporator/condenser (Fig. 4).

The dehydration was carried out at 140°C while hydration at 46°C, the condenser/evaporator was submerged in a thermal bath thermostated at 20°C which corresponds to the saturated water vapor pressure of ca. 23 mbar. The complete dehydration/hydration for all the material in the reactor was ensured by measuring the lost/gained weight during the experiment. Two beds of 20 tablets each were loaded into two separated compartments of the reactor which were stacked one upon another as shown in Fig. 4. In total, 50 hydration/dehydration cycles were carried out. After the cycling, the tablets from both compartments were carefully unloaded and photographed by means of digital camera Canon DS126431 (lens Tamron 60 mm R/2.0 Macro SP Di II) which was mounted on a calibrated measuring table Kaiser RS 2 CP. The photographs of the beds were processed by MATLAB. An ellipse with was drawn around each tablet and two measures were selected to judge about the tablet deformation after the cycling: the length of the longer axis of ellipse *a* and the aspect ratio of an ellipse, i.e. ratio of lengths of the longer and shorter axes (*a*/*b*).

Pressure drop measurements were performed for two beds of tablets (0.5 g, d = 12 mm) placed in two similar lab-scale tube reactors made of brass (d_{in} = 30 mm, height of the bed ~25–30 mm) with porous glass

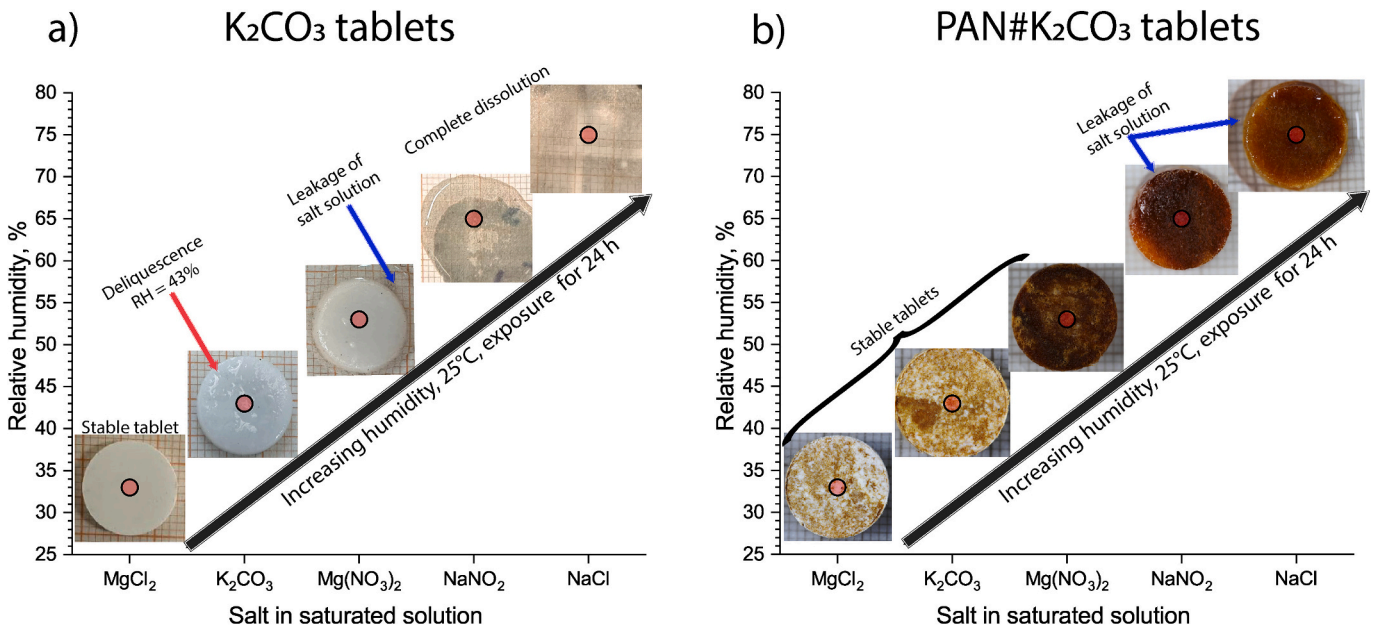

Fig. 9. The photographs of leakage tests of K_2CO_3#PAN tablets.

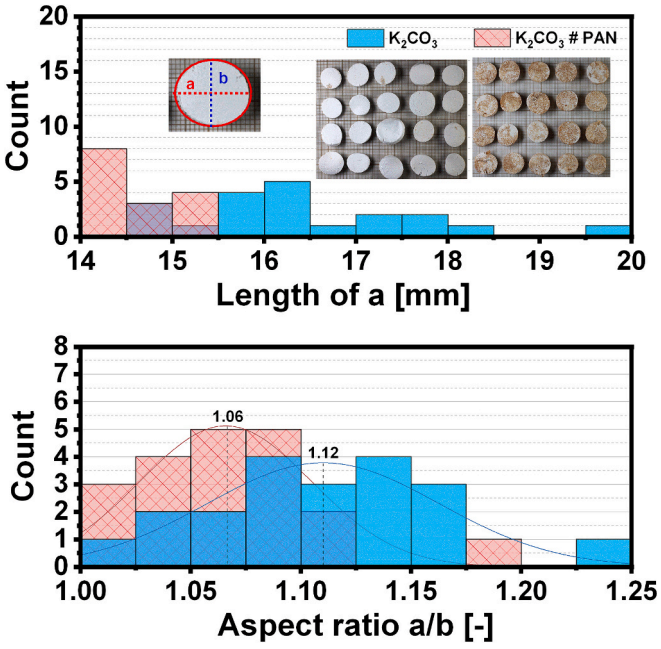

Fig. 10. Geometric parameters of the tablets after 50 cycles in beds and their original photographs put as an inset.

filters at the bottom. For each of the two reactors, a bed of 20 tablets (K_2CO_3 or K_2CO_3#PAN) was prepared. Both reactors were equipped with mass flow controllers and differential pressure drop sensors (Sensirion SDP810-500 Pa) allowing to measure the pressure drops at various flows of dry air (0.5–8.5 l/min). After the initial loading, the measured pressure drops of the beds were corrected by subtracting the pressure drops of empty reactors:

$$\Delta P_{bed} = \Delta P_{measured} - \Delta P_{empty} \quad (9)$$

After the initial pressure drop measurements, the reactors were put in the desiccator over $MgCl_2$ (25°C, RH = 33%, P ~ 10 mbar) for 8–10 h to ensure complete hydration. For dehydration, the reactors were put in an oven at 130°C overnight. Six such cycles were carried out, and after each hydration or dehydration the bed pressure drop was measured.

3. Results and discussion

3.1. Characterization of the tablets

The initial raw material before pressing consists of fibers of 12–15 μm in diameter (red arrows on Fig. 5a) loosely interspersed with irregularly shaped salt crystallites of 100–400 μm (blue arrows on Fig. 5a). Pressing of the raw material makes it denser, which can be observed on SEM images of the tablet surface consisting of closely packed salt crystallites with fibers in between (Fig. 5b). The fibers entangle the salt particles creating the bound structure visible on micro-CT scans (Fig. S4 provided in Supplementary Material).

The fibers are colored after pressing and the thermal treatment at 160°C (Fig. 5b and Fig. S2 provided in Supplementary Material), which is likely attributed to some cyclization of PAN yielding conjugated aromatic compounds causing the dark coloring [40]. Nonetheless, the PAN fibers are mechanically stable up to $T > 200$°C [41] and chemically up to 300°C with no traceable degradation under the conditions of a thermochemical cycle (Fig. S1 provided in Supplementary Material). The salt can be removed by gentle washing, leaving the residue consisting of intertwined fibers (Fig. 5c).

The reinforcing effect of fibers was tested by crushing the tablets. According to the results of the crushing tests (Fig. S5 provided in Supplementary Material), the mean initial slope of the elastic deformation region is higher for K_2CO_3#PAN than for K_2CO_3 tablets by a factor of 1.7, and the mean maximal force that a fiber-reinforced tablet can withstand is increased by a factor of ~2.5 (Fig. 6). This effect is likely to be attributed to a higher mechanical connectivity of the particles causing the reinforcement for other fiber composites [35].

The initial porosity of K_2CO_3#PAN is higher than the porosity of the fiber-free K_2CO_3 tablets suggesting that fiber network creates an extra empty space likely due to elastic relaxation of the fibers after pressing the tablets (Fig. 7). The porosity monotonously increases during cycling, reaching 38–39% for hydrated and ~ 52–54% for dehydrated tablets. Interestingly, the porosities of K_2CO_3 and K_2CO_3#PAN tablets become equal within the error range after one hydration/dehydration cycle and remain equal for the next four cycles both for hydrated and dehydrated tablets. The disappearance of the initial difference suggests that cycling

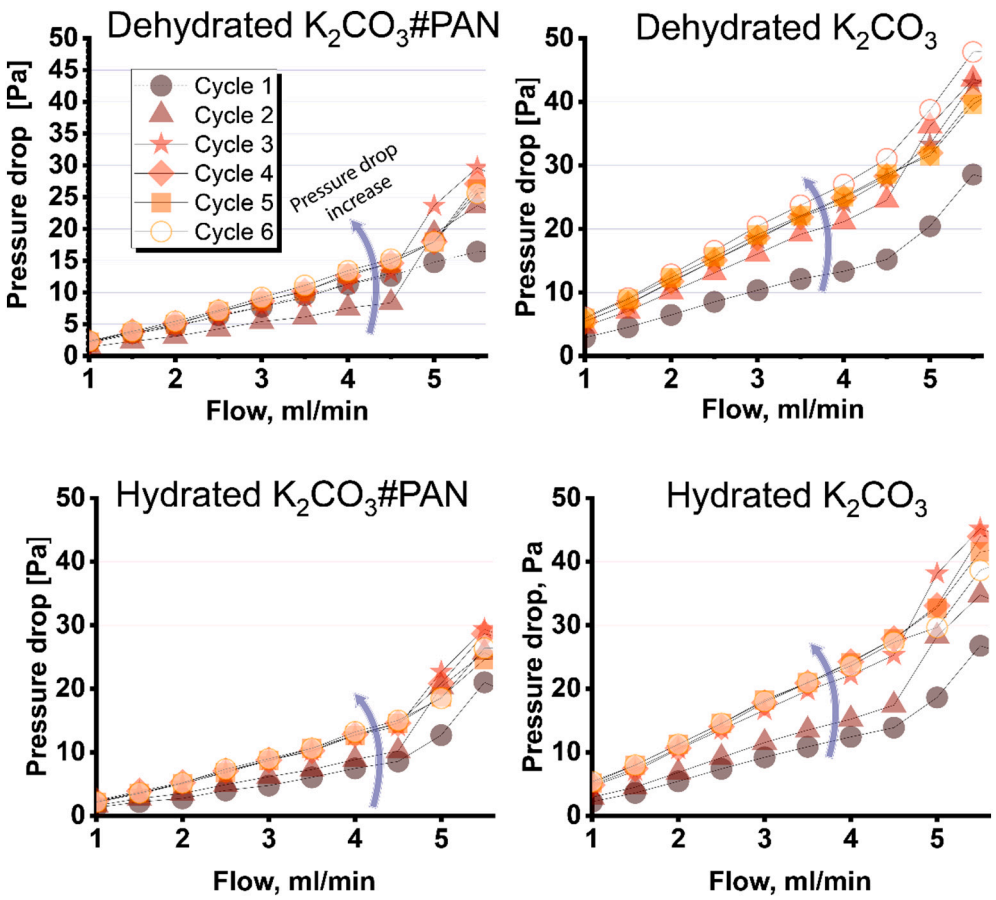

Fig. 11. Pressure drop evolution in the course of cycling for hydrated (top) and anhydrous (bottom) tablets of K_2CO_3 (left) and K_2CO_3#PAN (right).

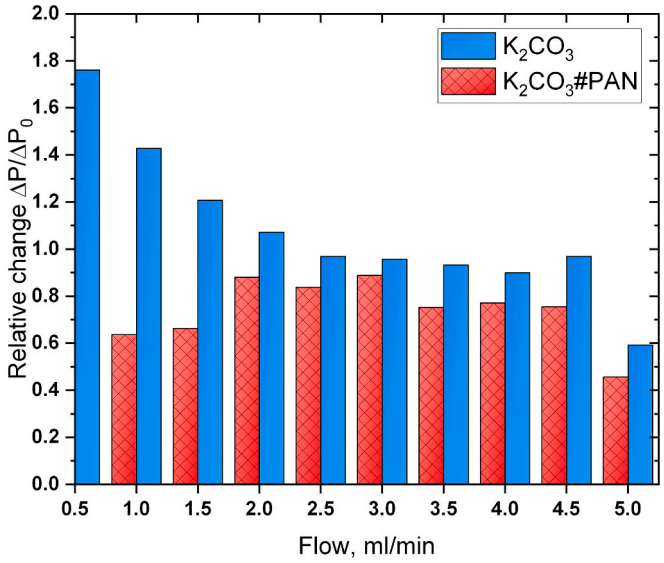

Fig. 12. Relative increase of pressure drop after five cycles for K_2CO_3 and K_2CO_3#PAN.

determines the porous microstructure of the cycled tablets stronger than the fibers additive or the preparation procedure.

The kinetic curves of dehydration suggest that fibers do not affect dehydration rate of the tablets at 130°C and ambient humidity (Fig. 8). At the same time, hydration conversion for tableted K_2CO_3 is somewhat lower than for K_2CO_3#PAN, reaching nearly 1 for all the tablets after 10 h of hydration (not shown). The hydration kinetics of tableted K_2CO_3 is governed by its porosity and the hydration rate is very sensitive to this parameter [42]. Speculatively, the difference may be explained by somewhat higher porosity for K_2CO_3#PAN tablets during the first two cycles.

Deliquescence may be a major problem for applications if the deliquescence relative humidity is inadvertently reached during a thermochemical cycle. The deliquescence relative humidity (RH) for K_2CO_3 is 43%, and after exposing a tablet of K_2CO_3 to this humidity for 24 h one can observe traces of salt solution on the tablets surface (Fig. 9a). As the relative humidity increases, the volume of the solution increases and its leakage is visible at RH = 53%. A further increase in RH leads to the complete dissolution of the tablets. The introduction of the fiber network mitigates the consequence of the deliquescence as the structure is capable of holding extra K_2CO_3 solution at least up to relative humidity of 53% (Fig. 9b). The leakage becomes apparent only at RH > 65%, and does not disintegrate the tablets.

In summary, the K_2CO_3#PAN tablets are composed of fibers (5.4 wt %) entangling salt particles of several hundred micrometers. The fibers dramatically improve mechanical properties of the tablets, slightly increase hydration rate while practically not affecting the tablet porosity and its evolution during cycling. The leakage tests suggest that K_2CO_3#PAN are stable with respect to leakage up to a relative humidity of 53%.

3.2. Bed tests

Two beds of 20 tablets each were cycled to highlight the effect of cycling on tablet deformation. After performing 50 cycles, the K_2CO_3 tablets were found to have more irregular shapes, whereas K_2CO_3#PAN tablets appeared to be less deformed. The visual comparison was

corroborated by image analysis approximating every tablet shape as an ellipse (Fig. 10). The average length of the longer axis a is higher for the tablets without fibers. Another measure of irregularity, that is the ratio of longer axis to the shorter one a/b, is also higher for the fiber-free tablets. Thus, both quantifiers suggest that fibers prevent irregular deformation of the tablets packed in a reactor bed and make the tablets more uniform after cycling.

The pressure drop measurements show that it increased nearly linearly with flow rate in the range of 0.5–4.5 l/min (Fig. 11), suggesting that the system was in the regime obeying the Darcy law. The permeability of the bed of K_2CO_3#PAN was found to be systematically higher than the one for K_2CO_3 tablets (Fig. S6 provided in Supplementary Material). The mechanical changes in the bed in the course of cycling cause the increase of the apparent pressure drop. This increase in pressure drop is however found to slow down when reaching cycle 5. It is also noteworthy, that for dehydrated K_2CO_3#PAN the pressure drop decreased after first cycle.

The relative increase in pressure drop is lower for the bed of fiber-reinforced tablets than for the bed without fibers at all flow rates (Fig. 12), likely due to the abovementioned mitigation of the irregular deformation of the tablets in the bed. The effect is less pronounced at high flow rates, however, in a real TCES device the desired flow rate is a subject of trade-off between power output and outlet temperature.

Thus, the fiber reinforcement technique retards the increase in pressure drop in a bed of centimeter-sized reactive tablets likely due to the more regular macroscopic deformation of the tablets in the bed. Therefore, the technique has the potential to be applied in thermochemical reactors filled with solid centimeter-sized particles of salt hydrates. We believe that the amelioration of tablets properties with fibers may be complementary with the modern reactor design approaches to improve the performance and cyclic behavior for thermochemical energy storage systems [43]. The preparation method involving mechanical treatment can potentially be further optimized to become scalable for domestic TCES systems. However, such optimization is beyond the scope of the present work.

4. Conclusions

In this work the stabilization of centimeter-sized salt hydrate reactive tablets by means of reinforcement with polymeric fibers is demonstrated and thoroughly investigated. The technique involving intense homogenization was shown suitable for preparation of the composite tablets consisting of polyacrylonitrile (PAN) fibers that entangle the K_2CO_3 particles, with low weight content of fibers (5.4%) only slightly affecting storage density. For tablets with fibers the increase of crushing strength by a factor of 2.3 and Young modulus by a factor of 1.7 was shown. The evolution of tablets porosity in the course of cycling was not affected by the presence fibers, and the dehydration/hydration kinetics is affected only slightly, the difference does not exceed 10%. The improved mechanical properties lead to less tablet deformation after 50 cycles dehydration/hydration cycles which is deemed to cause the lower build-up of the pressure drop in the lab-scale reactor beds tested in this work. Moreover, stability of the tablets with respect to deliquescent conditions was shown to be improved, with the fiber-reinforced composites being stable up to 53% of relative humidity after 24 hours of exposure. Thus, fiber reinforcement may be a promising and inexpensive way to stable composite particles for future thermochemical energy storage reactors. The scalability of the proposed approach should be improved in the future by optimizing the preparation methodology, for example, by including industry-relevant methods such as electrospinning or impregnation.

CRediT authorship contribution statement

A. Shkatulov: Writing – review & editing, Writing – original draft, Visualization, Validation, Methodology, Investigation, Formal analysis, Conceptualization. **E. Averina:** Validation, Investigation, Formal analysis. **T. Raemaekers:** Writing – review & editing, Investigation, Formal analysis. **H. Fischer:** Writing – review & editing, Supervision, Funding acquisition, Conceptualization. **O.C.G. Adan:** Supervision, Project administration, Funding acquisition. **H. Huinink:** Writing – review & editing, Supervision, Resources, Project administration, Methodology, Funding acquisition, Conceptualization.

Declaration of competing interest

The authors declare the following financial interests/personal relationships which may be considered as potential competing interests: H.P. Huinink reports financial support was provided by Ministry of Economic Affairs and Climate Policy. H.P. Huinink reports financial support was provided by European Union. If there are other authors, they declare that they have no known competing financial interests or personal relationships that could have appeared to influence the work reported in this paper.

Data availability

Data will be made available on request.

Acknowledgements

This project has received funding from the European Union Horizon 2020 research and innovation program under grant agreement No 869810. This work reflects only the author's view. The European Commission is not responsible for any use that may be made of this information. Furthermore, funding has been received from the Ministry of Economic Affairs and Climate Policy for MOOI IWP project.

Appendix A. Supplementary data

Supplementary data to this article can be found online at https://doi.org/10.1016/j.est.2024.113764.

References

[1] THE 17 GOALS, Sustainable development. https://sdgs.un.org/goals (accessed September 2, 2024).
[2] W. Van Helden, Compact thermal energy storage, IEA SHC Task 67 (2023), https://doi.org/10.18777/ieashc-task67-2023-0001.
[3] Heating - fuels & technologies, IEA. https://www.iea.org/fuels-and-technologies/heating (accessed September 2, 2024).
[4] H.G. Kamath, R. Majumdar, A.V. Krishnan, R. Srikanth, Cost and environmental benefits of coal-concentrated solar power (CSP) hybridization in India, Energy 240 (2022) 122805, https://doi.org/10.1016/j.energy.2021.122805.
[5] L. Gur, K. Sawyer, R. Prasher, Searching for a better thermal battery, Science 335 (2012) 1454–1455.
[6] J. Stengler, M. Linder, Thermal energy storage combined with a temperature boost: an underestimated feature of thermochemical systems, Appl. Energy 262 (2020) 114530, https://doi.org/10.1016/j.apenergy.2020.114530.
[7] A.S. Pujari, R. Majumdar, S.K. Saha, C. Subramaniam, Annular vertical cylindrical thermochemical storage system with innovative flow arrangements for improved heat dispatch towards space heating requirements, Renew. Energy 217 (2023) 119168, https://doi.org/10.1016/j.renene.2023.119168.
[8] Z. Zeng, B. Zhao, R. Wang, Water based adsorption thermal battery: sorption mechanisms and applications, Energy Storage Mater. 54 (2023) 794–821, https://doi.org/10.1016/j.ensm.2022.11.024.
[9] Z. Ding, W. Wu, Type II absorption thermal battery for temperature upgrading: energy storage heat transformer, Appl. Energy (2022) 324, https://doi.org/10.1016/j.apenergy.2022.119748.
[10] P.A.J. Donkers, L.C. Sögütoglu, H.P. Huinink, H.R. Fischer, O.C.G. Adan, A review of salt hydrates for seasonal heat storage in domestic applications, Appl. Energy 199 (2017) 45–68, https://doi.org/10.1016/j.apenergy.2017.04.080.
[11] S. Kiyabu, P. Girard, D.J. Siegel, Discovery of salt hydrates for thermal energy storage, J. Am. Chem. Soc. 144 (2022) 21617–21627, https://doi.org/10.1021/jacs.2c08993.
[12] N. Mazur, M.A.R. Blijlevens, R. Ruliaman, H. Fischer, P. Donkers, H. Meekes, et al., Revisiting salt hydrate selection for domestic heat storage applications, Renew. Energy (2023) 119331, https://doi.org/10.1016/j.renene.2023.119331.

[13] M. Richter, E.-M. Habermann, E. Siebecke, M. Linder, A systematic screening of salt hydrates as materials for a thermochemical heat transformer, Thermochim. Acta 659 (2018) 136–150, https://doi.org/10.1016/j.tca.2017.06.011.
[14] M. Deutsch, D. Müller, C. Aumeyr, C. Jordan, C. Gierl-Mayer, P. Weinberger, et al., Systematic search algorithm for potential thermochemical energy storage systems, Appl. Energy 183 (2016) 113–120, https://doi.org/10.1016/j.apenergy.2016.08.142.
[15] K.E. N'Tsoukpoe, T. Schmidt, H.U. Rammelberg, B.A. Watts, W.K.L. Ruck, A systematic multi-step screening of numerous salt hydrates for low temperature thermochemical energy storage, Appl. Energy 124 (2014) 1–16, https://doi.org/10.1016/j.apenergy.2014.02.053.
[16] R.-J. Clark, G. Gholamibozanjani, J. Woods, S. Kaur, A. Odukomaiya, S. Al-Hallaj, et al., Experimental screening of salt hydrates for thermochemical energy storage for building heating application, J. Energy Storage 51 (2022) 104415, https://doi.org/10.1016/j.est.2022.104415.
[17] W. Kooijman, D.J. Kok, M.A.R. Blijlevens, H. Meekes, E. Vlieg, Screening double salt sulfate hydrates for application in thermochemical heat storage, J. Energy Storage 55 (2022) 105459, https://doi.org/10.1016/j.est.2022.105459.
[18] H. Huinink, S. de Jong, V. Houben, Hydration fronts in packed particle beds of salt hydrates: implications for heat storage, J. Energy Storage 71 (2023) 108158, https://doi.org/10.1016/j.est.2023.108158.
[19] A. Cosquillo Mejia, S. Afflerbach, M. Linder, M. Schmidt, Experimental analysis of encapsulated CaO/ca(OH)2 granules as thermochemical storage in a novel moving bed reactor, Appl. Therm. Eng. 169 (2020) 114961, https://doi.org/10.1016/j.applthermaleng.2020.114961.
[20] V. Brancato, L.G. Gordeeva, A.D. Grekova, A. Sapienza, S. Vasta, A. Frazzica, et al., Water adsorption equilibrium and dynamics of LICL/MWCNT/PVA composite for adsorptive heat storage, Sol. Energy Mater. Sol. Cells 193 (2019) 133–140, https://doi.org/10.1016/j.solmat.2019.01.001.
[21] Y.I. Aristov (Ed.), Nanocomposite Sorbents for Multiple Applications, 1 edition, Jenny Stanford Publishing, 2020.
[22] C.T. Oguchi, S. Yu, A review of theoretical salt weathering studies for stone heritage, Prog Earth Planet Sci 8 (2021) 32, https://doi.org/10.1186/s40645-021-00414-x.
[23] J. Aarts, H. Fischer, O. Adan, H. Huinink, Impact of cycling on the performance of mm-sized salt hydrate particles, J. Energy Storage 76 (2024) 109806, https://doi.org/10.1016/j.est.2023.109806.
[24] Z. Fan, Y. Zhao, X. Liu, Y. Shi, D. Jiang, Development of a new composite material for building energy storage based on lauric acid-palmitic acid-paraffin ternary eutectic and expanded perlite, J. Energy Storage (2022) 53, https://doi.org/10.1016/j.est.2022.105136.
[25] A.I. Shkatulov, J. Houben, H. Fischer, H.P. Huinink, Stabilization of K2CO3 in vermiculite for thermochemical energy storage, Renew. Energy 150 (2020) 990–1000, https://doi.org/10.1016/j.renene.2019.11.119.
[26] N. Xie, X. Gao, Y. Zhong, R. Ye, S. Chen, L. Ding, et al., Enhanced thermal performance of Na2HPO4·12H2O composite phase change material supported by sepiolite fiber for floor radiant heating system, J. Build. Eng. (2022) 56, https://doi.org/10.1016/j.jobe.2022.104747.
[27] E. Courbon, P. D'Ans, A. Permyakova, O. Skrylnyk, N. Steunou, M. Degrez, et al., A new composite sorbent based on SrBr2 and silica gel for solar energy storage application with high energy storage density and stability, Appl. Energy 190 (2017) 1184–1194, https://doi.org/10.1016/j.apenergy.2017.01.041.
[28] A. Jabbari-Hichri, S. Bennici, A. Auroux, CaCl 2 -containing composites as thermochemical heat storage materials, Sol. Energy Mater. Sol. Cells 172 (2017) 177–185, https://doi.org/10.1016/j.solmat.2017.07.037.
[29] V. Brancato, L. Calabrese, V. Palomba, A. Frazzica, M. Fullana-Puig, A. Solé, et al., MgSO4·7H2O filled macro cellular foams: an innovative composite sorbent for thermo-chemical energy storage applications for solar buildings, Sol. Energy 173 (2018) 1278–1286, https://doi.org/10.1016/j.solener.2018.08.075.
[30] J. Aarts, B. van Ravensteijn, H. Fischer, O. Adan, H. Huinink, Polymeric stabilization of salt hydrates for thermochemical energy storage, Appl. Energy 341 (2023) 121068, https://doi.org/10.1016/j.apenergy.2023.121068.
[31] A. Mehari, Z.Y. Xu, R.Z. Wang, Thermodynamic evaluation of three-phase absorption thermal storage in humid air with energy storage density over 600 kWh/m3, Energ. Conver. Manage. 258 (2022) 115476, https://doi.org/10.1016/j.enconman.2022.115476.
[32] A. Shkatulov, R. Joosten, H. Fischer, H. Huinink, Core–shell encapsulation of salt hydrates into mesoporous silica shells for thermochemical energy storage, ACS Appl. Energy Mater. 3 (2020) 6860–6869, https://doi.org/10.1021/acsaem.0c00971.
[33] A. Shkatulov, L.G. Gordeeva, I.S. Girnik, H. Huinink, Y.I. Aristov, Novel adsorption method for moisture and heat recuperation in ventilation: composites "LiCl/matrix" tailored for cold climate, Energy 201 (2020) 117595, https://doi.org/10.1016/j.energy.2020.117595.
[34] J. Sim, C. Park, D.Y. Moon, Characteristics of basalt fiber as a strengthening material for concrete structures, Compos. Part B Eng. 36 (2005) 504–512, https://doi.org/10.1016/j.compositesb.2005.02.002.
[35] B. Shafei, M. Kazemian, M. Dopko, M. Najimi, State-of-the-art review of capabilities and limitations of polymer and glass fibers used for Fiber-reinforced concrete, Materials 14 (2021) 409, https://doi.org/10.3390/ma14020409.
[36] L.C. Sögütoglu, P.A.J. Donkers, H.R. Fischer, H.P. Huinink, O.C.G. Adan, In-depth investigation of thermochemical performance in a heat battery: cyclic analysis of K 2 CO 3, MgCl 2 and Na 2 S, Appl. Energy 215 (2018) 159–173, https://doi.org/10.1016/j.apenergy.2018.01.083.
[37] J. Wang, R. Zhang, L. Lu, Q. Luo, X. Li, Y. Yi, et al., Evaluation of mechanical properties and abrasion resistance of PAN fiber-reinforced sulfoaluminate cement composites, Case Stud. Constr. Mater. 18 (2023) e01973, https://doi.org/10.1016/j.cscm.2023.e01973.
[38] L. Greenspan, Humidity fixed points of binary saturated aqueous solutions, J. Res. Natl. Bureau Stand. Sect. A: Phys. Chem. 81A (1977) 89, https://doi.org/10.6028/jres.081A.011.
[39] J. Houben, A. Shkatulov, H. Huinink, H. Fischer, O. Adan, Caesium doping accelerates the hydration rate of potassium carbonate in thermal energy storage, Sol. Energy Mater. Sol. Cells (2023) 251, https://doi.org/10.1016/j.solmat.2022.112116.
[40] T. Usami, T. Itoh, H. Ohtani, S. Tsuge, Structural study of polyacrylonitrile fibers during oxidative thermal degradation by pyrolysis-gas chromatography, solid-state carbon-13 NMR, and Fourier-transform infrared spectroscopy, Macromolecules 23 (1990) 2460–2465, https://doi.org/10.1021/ma00211a009.
[41] K. Sen, P. Bajaj, T.V. Sreekumar, Thermal behavior of drawn acrylic fibers, J Polym Sci B 41 (2003) 2949–2958, https://doi.org/10.1002/polb.10609.
[42] J. Aarts, S. de Jong, M. Cotti, P. Donkers, H. Fischer, O. Adan, et al., Diffusion limited hydration kinetics of millimeter sized salt hydrate particles for thermochemical heat storage, J. Energy Storage 47 (2022) 103554, https://doi.org/10.1016/j.est.2021.103554.
[43] A.S. Pujari, R. Majumdar, C. Subramaniam, S.K. Saha, Study of Different Flow Configurations of Radial Flow Annular Reactor for Thermochemical Energy Storage. Proceeding of Proceedings of the 27th National and 5th International ISHMT-ASTFE Heat and Mass Transfer Conference December 14–17, 2023, IIT Patna, Patna-801106, Bihar, India, Bihar, India: Begellhouse, 2024, pp. 821–826, https://doi.org/10.1615/IHMTC-2023.1330.